Available online at www.sciencedirect.com
SCIENCE DIRECT®
Journal of Sound and Vibration 282 (2005) 197–214
JOURNAL OF SOUND AND VIBRATION
www.elsevier.com/locate/jsvi

Vibration suppression of stepped beams: new designs for hot-wire probes

C.S. Anderson, S.E. Semercigil*, Ö.F. Turan

School of the Built Environment Mechanical Engineering, Victoria University of Technology, P.O. Box 14428, MCMC, Melbourne, Vic. 8001, Australia

Received 1 October 2001; received in revised form 11 February 2004; accepted 18 February 2004

Abstract

Local geometric modifications to slender stepped-beam structures are presented to minimise dynamic response under broadband excitation. The particular application in this paper is the sensing wire of a hot-wire probe. Hot-wire anemometry is an experimental technique to measure instantaneous velocity and temperature fluctuations in flows. The sensing wire of the probe is a thin wire. It is prone to large amplitude resonance vibrations when exposed to turbulent flow, which may cause significant errors in measurements. Therefore, minimising resonance vibrations of the wire should improve the accuracy of measurements. To this end, numerical predictions and laboratory measurements with a scaled model are presented. Currently, flow measurements are being taken to demonstrate the accuracy due to the proposed structural modifications. The method also holds promise for other problems where it is possible to manipulate the spectral distribution of natural frequencies.

1. Introduction

Hot-wire anemometry is a powerful and practical technique for measuring mean and fluctuating fluid velocities and temperatures in turbulent flows. It is relatively inexpensive and easy to use for research, teaching and industrial applications. For traditional isothermal applications,

*Corresponding author. Tel.: +61-3-9688-4009; fax: +61-3-9688-4139.
E-mail address: Eren.Semercigil@vu.edu.au (S.E. Semercigil).

0022-460X/$ - see front matter © 2004 Elsevier Ltd. All rights reserved.
doi:10.1016/j.jsv.2004.02.025

the sensor of a hot-wire probe, which is a thin wire, is kept at a temperature of about 300 °C during measurements. This mode of operation is referred as the constant temperature anemometry (CTA) mode. The thin wire can be in the order of 2–6 μm in diameter and about 1–3 mm in length. In Figs. 1(a) and (b), respectively, a typical hot-wire probe and its sensing wire are presented. In Fig. 1(c), a photograph is given to show the boundary condition where the wire is attached to the prong.

In hot-wire anemometry, the cooling effect of the oncoming fluid on the sensing wire is interpreted as the flow velocity to be measured. The underlying assumption of this interpretation is that the wire is stationary, and the velocity of the flow 'relative' to the wire can be assumed to be the 'absolute' flow velocity. However, due to its flexibility, the probe wire is susceptible to large amplitude resonance vibrations. As a result of these vibrations, the relative velocity can no longer represent a close indication of the absolute flow velocity.

The problem of wire vibration was first observed by Perry and Morrison [3,4]. These workers investigated rotational vibration and skipping (or whirling) of the wire. However, the more predominant case of stream-wise transverse vibrations had not been investigated in detail before the work of Turan et al. [2].

Turan et al. [2] reported measurement errors when large amplitude wire vibrations are expected. It is suggested that the filament of a hot-wire probe can be excited at its first or higher resonance modes. If the probe wire is excited in the first mode, the resulting vibration velocity is in-phase with the velocity fluctuations in the flow along the entire wire length. Hence, these in-phase oscillations may reduce the relative velocity between the wire and the flow, leading to smaller readings than the true velocity of the flow. Therefore, hot-wire dimensions must be chosen such that the resulting first natural frequency of the wire is higher than the expected frequency content in the flow.

One way to achieve a high first natural frequency of the wire is to use a short wire, which increases the dynamic rigidity. However, a short wire can have excessive heat loss to its prongs through conduction. Heat conduction creates a non-uniform temperature distribution along the wire, which in turn reduces measurement sensitivity. Hence, this condition is not acceptable. The

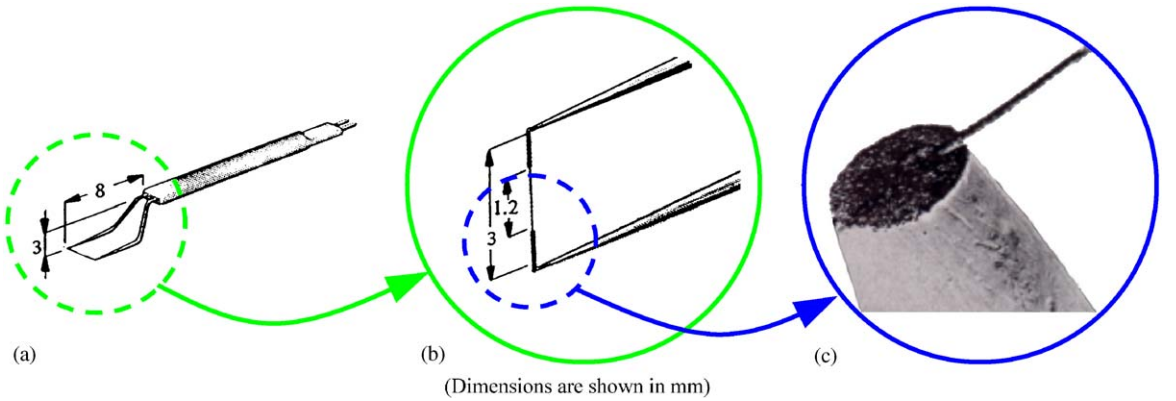

Fig. 1. Showing (a) hot-wire probe in entirety, (b) probe wire [1], and (c) electron microscope photograph of wire and prong connection [2]. Dimensions are shown in mm.

problem of heat loss is discussed in Refs. [5,6]. To reduce heat loss to the prongs, an acceptable sensitive length, L, had been defined as $L/d \geqslant 200$ [5] where d is the sensing wire diameter. This definition was later modified to $160 \leqslant L/d \leqslant 310$ [7]. The upper limit is to minimise spatial averaging of eddies with short-wave length over the wire length.

In Ref. [2], a limited number of already existing favourable designs were identified. However, no effort was made to search for new designs. The objective of the present study is to suggest geometric changes that can yield improved dynamic characteristics. The following section briefly describes the proposed control strategy. Then, the numerical model and numerical predictions are presented using a standard finite element procedure in Sections 3–5. Experiments with scaled prototype models of the typical designs, and comparison of the experimental observations and numerical predictions are given in Sections 6 and 7.

2. Proposed technique

Investigation by the authors demonstrated that when the first and second resonance frequencies were close, beam structures had favourable vibration characteristics [8,9]. The reason for this trend can be related to the particular shape that a beam assumes when excited at a resonance frequency. In Fig. 2, the first two mode shapes of a fixed-fixed, uniform beam are shown. The second resonance mode has a point of zero amplitude at the mid-span, whereas the first resonance mode has a point of maximum amplitude. When the first two natural frequencies are close, these two mode shapes should have equal opportunity to contribute to the response of the beam.

In Fig. 2(c), the same beam is shown with a shape obtained by averaging the first two mode shapes, assuming that both have identical contribution. The resulting shape has a node at about $\frac{1}{3}$ distance from one end, on the side where the second mode happens to be out-of-phase with the first mode. This node, however, is unstable since the value of the second natural frequency will always be somewhat larger than that of the first natural frequency. As a result, the node will travel towards the middle, and then to the other side of the beam, before it turns back to assume the location shown in the figure.

If a beam is designed to have virtually coincident natural frequencies of the first two modes, then neither of the two natural modes will be able to establish itself. For such a design, response of the more critical fundamental mode will be effectively suppressed by the node of the second mode. The objective of this study is to achieve close first two natural frequencies by making local structural changes.

It should be emphasised that Fig. 2 (c) is included here only to clarify the objective of this study. The critical modes of a uniform cross-sectioned beam are well separated from each other, with no possibility for the co-existence of the first two modes. In fact, a stepped geometry, rather than a uniform one, appears to be one way of achieving close natural frequencies (mode shapes corresponding to a stepped geometry are presented later in Fig. 9).

An example of wire vibration is given in Fig. 2(d) and (e) from the authors' own measurements. These measurements were taken 20 mm outside the exit of a fully developed turbulent pipe flow with a Reynolds number of 230,000, 13.2 mm radially inward from the wall of the 108-mm diameter pipe. Here, the Reynolds number is defined as follows: $Re = U_{\text{ave}}d/\nu$, where U_{ave} and d are the average velocity in the pipe and its inner diameter, respectively, and ν is the kinematic

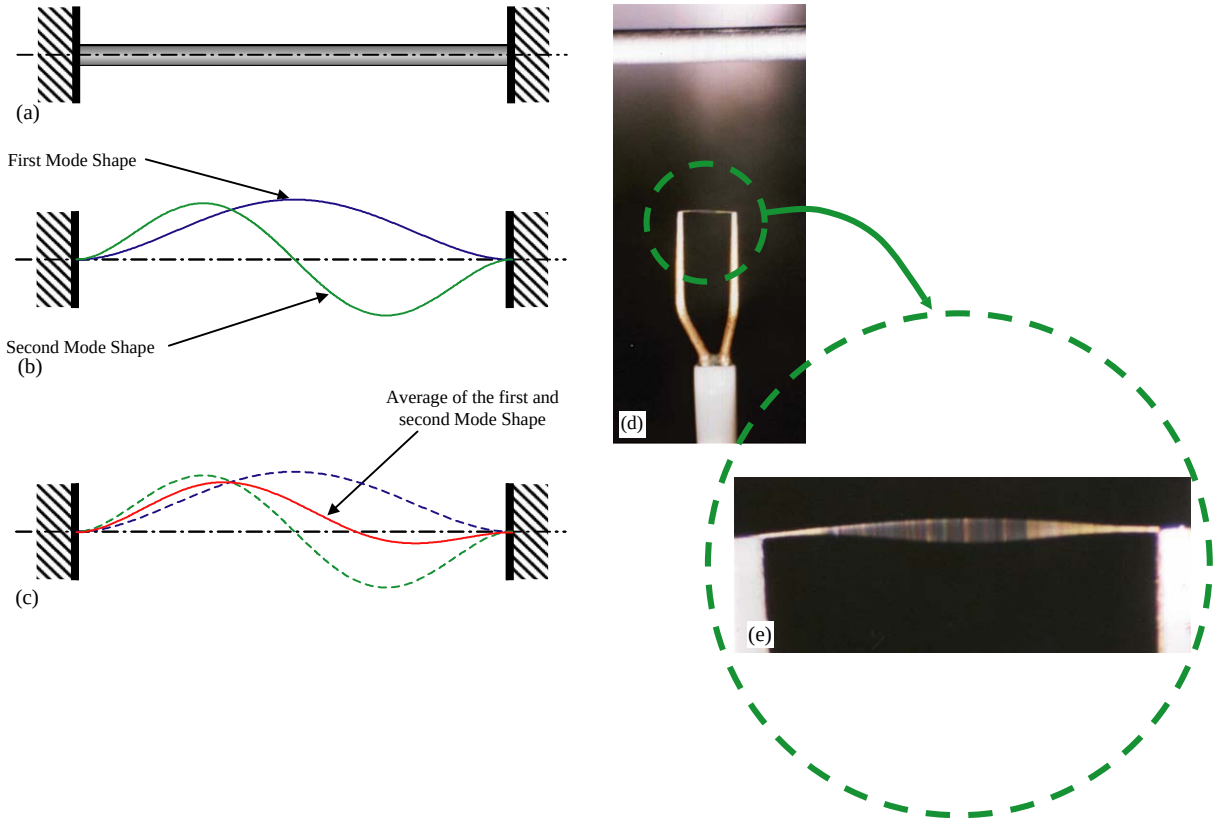

Fig. 2. (a) The fixed–fixed beam model, (b) its first two mode shapes and (c) the first two mode shapes with their average, (d) Probe 3 in the wake of a 2-mm diameter cylinder and (e) close-up of the sensing wire.

viscosity of the fluid (air). The photograph shows a top view where the flow direction is from the top to bottom of the frame. Following the schematic representation in Fig. 3, the hot wire had a total length of $L_o = 3\,\text{mm}$, sensing length and diameter, respectively, of $L = 1.10\,\text{mm}$ and $d = 5.75\,\mu\text{m}$, and end diameter of $d_g = 40\,\mu\text{m}$. Consequently, its first two natural frequencies were 12,200 and 12,800 Hz (the procedure for predicting natural frequencies is presented in the next section). These conditions, in the wake of a 2-mm diameter cylinder, provided sufficient excitation for the wire to clearly exhibit the first mode shape indicated by the blurred envelope [10].

3. Numerical model

For numerical modelling purposes, the hot-wire is represented as shown in Fig. 3. In this figure, the middle sensing wire has d and L for diameter and length, whereas d_g, L_g and L_o represent the diameter and the length of the thicker ends and the total length of the wire, respectively. Boundary conditions are taken to be built-in where the wire is welded to the prongs. The electron microscope photograph presented in Fig. 1(c), justifies this boundary condition due to the welded

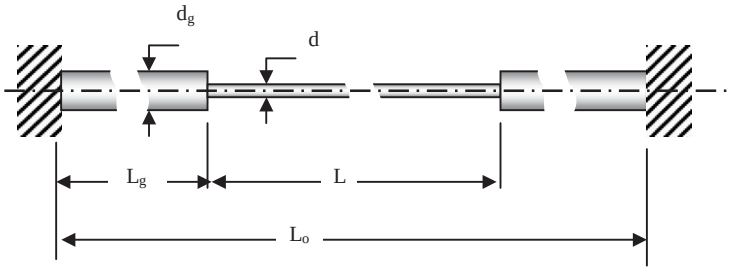

Fig. 3. Schematic representation of the probe wire used for numerical modelling.

connections. Hot-wire probes are manufactured with an intentional pre-tension at room temperature. The numerical model does not include this pre-tension. The presence of any wire pre-tension would simply increase all the natural frequencies by the same scale, rather than making any relative changes. In addition, pre-tension is mostly lost when the wire is heated for flow measurements.

Along the length of the wire, 30 standard finite beam elements [11] were used to approximate the dynamic properties of the model in Fig. 3. The three sections of the beam had ten elements each, a sufficient number to give an accurate representation of the first five mode shapes. Solution of the resulting eigenvalue problem in Matlab [12] provided the first 58 natural frequencies for the wire, of which the first five were of interest, since the higher modes are well outside the frequency range of flow excitation.

Dynamic response of the wire to a broadband, random white noise excitation force was obtained by numerically integrating the system differential equations of motion using the Newmark-β technique [11]. The frequency content of the excitation force (zero to 50 kHz) was sufficient to excite up to the fifth mode of the wire. This external force was applied at one node to the right of the mid-point so as to be able to excite the even numbered modes which have nodes at the mid-point. Fifty thousand steps of integrations were performed with a time step of 10 μs to allow the root mean square (rms) of the displacement to settle to within 1% of its steady-state value.

One of the existing hot-wire probe geometries, Probe 3 in Ref. [2], is investigated here as the starting geometry. This probe has a total length of 3 mm, a sensitive length and diameter of 1.18 and 5.75 μm, respectively, resulting in a sensitive length to diameter ratio, L/d, of 205. It has a thick end diameter of 30 μm. The probe wire has a platinum core plated with tungsten, and its thicker ends are coated with gold. Probe 3 was found to be the least susceptible to large amplitude vibrations, and one of the most accurate for measurements in turbulent flow [13]. The objective here is to possibly improve it further.

4. Numerical predictions

The effect of varying the ratio of the length of the end sections to the sensitive length, L_g/L, is shown in Fig. 4. From left to right along the horizontal axis, the ratio of the end length to the sensitive length, L_g/L, increases. For a constant L_o of 3 mm, this increase results in a shorter L

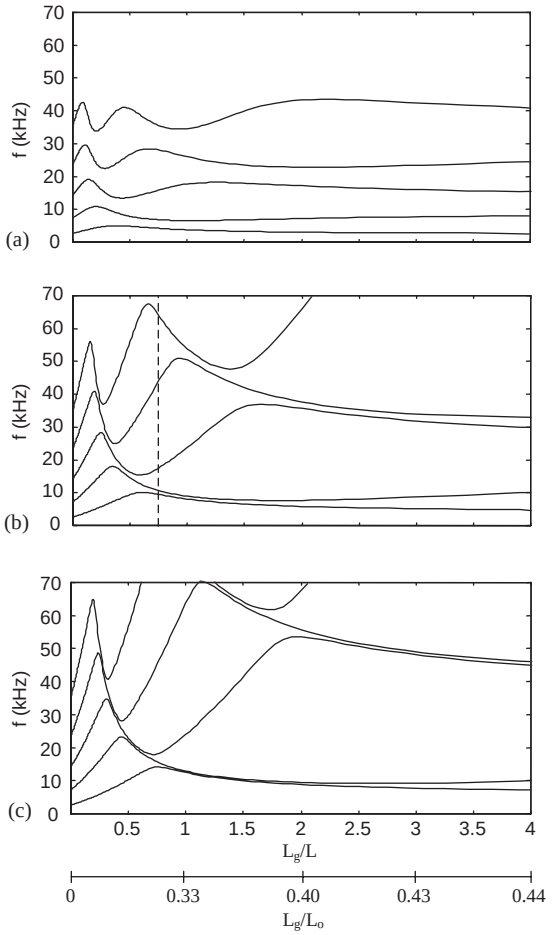

Fig. 4. Variation of the first five natural frequencies with L_g/L for d_g of (a) 15 μm, (b) 30 μm and (c) 45 μm. L_g/L_o scale also shown.

and longer L_g since $L_o = 2L_g + L$. The ratio of the end length to the total length, L_g/L_o, is also shown as a second axis for reference. The vertical axis represents the five resonance frequencies of the wire, f_{n1} to f_{n5}, corresponding to the five curves given in ascending order. Figs. 4(a)–(c) correspond to end diameters, d_g, of 15, 30 and 45 μm, respectively.

The starting geometry of Probe 3 is marked with a vertical dashed line at the original value of L_g/L of 0.77 in Fig. 4(b). As L_g/L increases from the starting value of 0.77 in this figure, the first and second resonance frequencies become similar, while the third resonance frequency is pushed away. Furthermore, the third and fourth resonance frequencies also approach one another as L_g/L increases. As the thick ends increase in length, they become more flexible and participate more actively in vibrations. It appears that thick ends can participate a lot more readily in the first two modes as compared to the higher ones. As a result, increasing L_g/L generally gives smaller f_{n1} and f_{n2}, while higher modes can exhibit initial rapid increases before leveling off and decreasing

gradually. This trend is most clearly observed in Fig. 4(c), where d_g is 45 μm, whereas Fig. 4(a) shows only slight changes in the relative positioning of natural frequencies.

The effect of L_g/L decreasing from the starting value of 0.77 is the relative separation of the resonance frequencies. For a L_g/L of approximately 0.2, all five resonance frequencies become almost equally spaced. The reason for this trend originates from the effective stiffening of the ends as they become shorter. Short ends contribute less to the dynamic response. The response of the sensing wire overwhelms that of the thick ends, eventually approaching the case of a uniform beam consisting of the sensing section alone with well separated natural frequencies.

Eight representative end length to sensitive length ratios (of 0.5, 0.77, 1, 1.13, 1.5, 2, 2.5 and 3) were chosen from Fig. 4 and subjected numerically to a random white noise excitation to obtain their dynamic response for comparison. The results of this excitation are shown in Fig. 5. In Fig. 5, a value of zero on the horizontal axis represents the middle of the wire. The vertical axis is the normalized rms of the response amplitude due to the excitation force. The vertical axis is normalized by dividing the rms response of each case by the rms response (in the mid span) of Probe 3, of Ref. [2]. Hence, any new probe with a normalised rms response smaller than unity represents a desirable structural improvement. Any normalised response larger than unity, however, indicates a detrimental effect due to geometric changes. Probe 3 is marked with (o) in Fig. 5 (b), having a L_g/L of 0.77, with a total length of 3 mm and an end diameter, d_g of 30 μm.

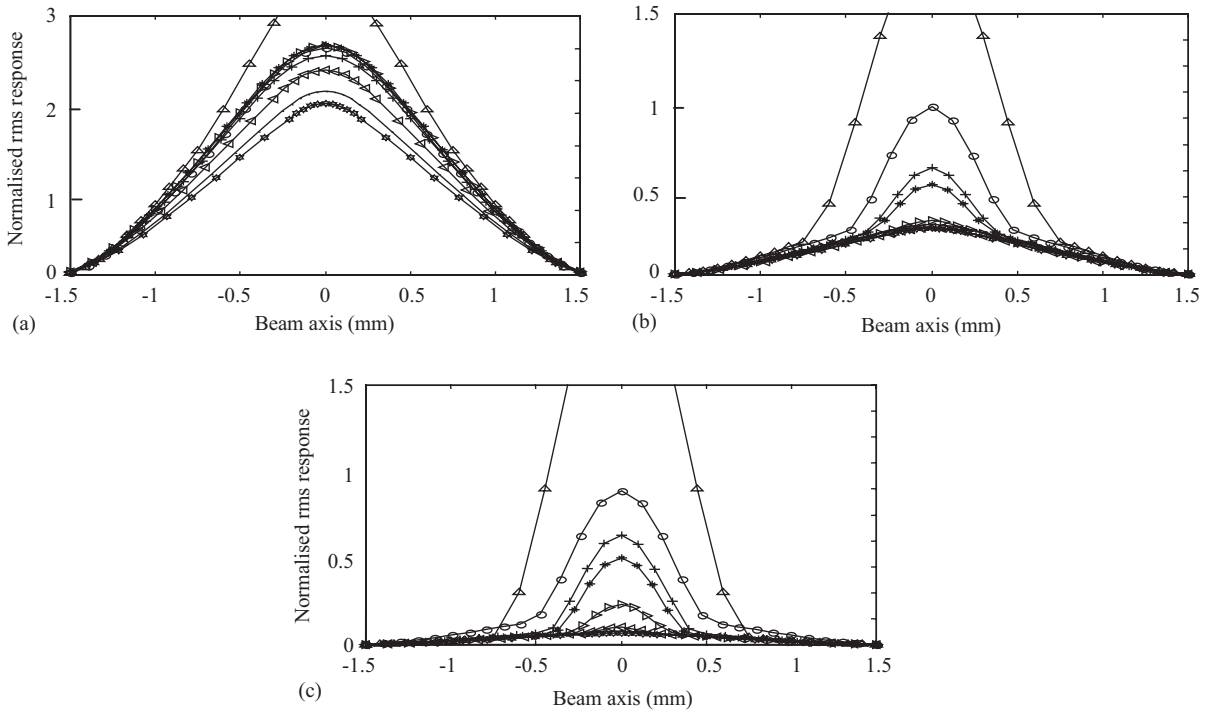

Fig. 5. Variation of the normalised rms displacement response for random white noise excitation and for d_g of (a) 15 μm, (b) 30 μm and (c) 45 μm. L_g/L: 0.5(△); 0.77(o); 1(+); 1.13(*); 1.5(▷); 2(◁); 2.5(●); 3(✡).

Clearly, reduction in the end diameter to 15 μm, has a detrimental effect as shown by the increased rms amplitudes in Fig. 5(a). Fig. 5(b) shows the reduction in amplitude achievable by altering only L_g/L. The best, lowest amplitude, case is for a L_g/L of 3 (✡). It is notable, however, that there is little difference in amplitude between geometries having a L_g/L of between 1.5 (▷) and 3 (✡). Fig. 5(c) shows the rms amplitudes for probes with an increased end diameter d_g of 45 μm. Here, a probe with L_g/L of 1.5 (▷) has comparable amplitude to that having L_g/L of 1.5 (▷) with d_g of 30 μm. However, unlike the case for 30 μm, increasing L_g/L to 3 (✡), reduces the rms amplitude significantly for 45 μm.

A more concise presentation of this data may be achieved by plotting only the mid-span rms amplitude for each geometry, as shown in Fig. 6. Similar to Fig. 5, the rms responses are normalised by dividing them by the response of the starting geometry. The horizontal dotted line represents the rms response of Probe 3, which intersects the 30 μm line at a L_g/L of 0.77. Fig. 6 shows clear reduction of rms amplitude as L_g/L increases. Of particular interest is the plateau seen in the curves corresponding to end diameters, d_g, of 30 and 45 μm.

The displacement history of Probe 3 is shown in Fig. 7, along with those of two better cases having L_g/L of 2 and d_g of 30 μm (Probe A) and 45 μm (Probe B) chosen from Fig. 6. Here, the vertical axes are normalised by scaling the peak response of Probe 3 in Fig. 7(a) as unity. The displacement histories show the reduction in response due to the suggested geometric changes. The smallest rms amplitude, approximately 0.1 in Fig. 6, is achieved using a total length of 3 mm, a L_g/L of 2 and an end diameter, d_g of 45 μm, referred as Probe B above. This combination represents a 90% reduction when compared to the original rms amplitude. The suggested geometric changes are shown graphically for clarity in Fig. 8, providing a visual comparison amongst Probes 3, A and B.

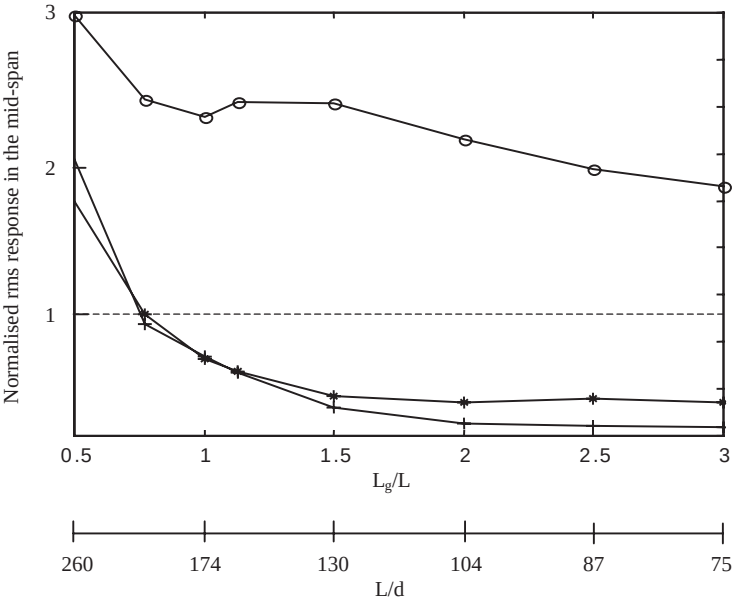

Fig. 6. Variation of the peak rms with L_g/L (or L/d) for d_g of 15 μm (o), 30 μm (*) and 45 μm (+).

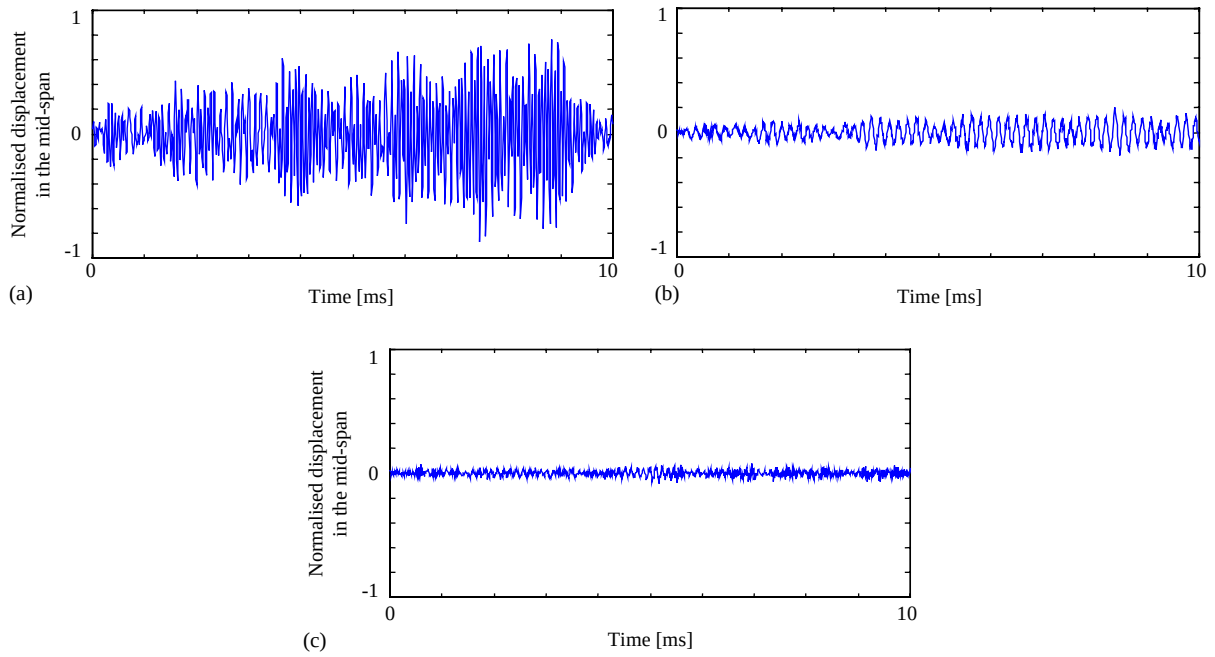

Fig. 7. Displacement histories for (a) Probe 3, (b) Probe A with $L_g/L=2$ and $d_g=30\,\mu m$, and (c) Probe B with $L_g/L=2$ and $d_g=45\,\mu m$. The sensitive length-to-diameter ratios for (a), (b) and (c) are 205, 104 and 104, respectively.

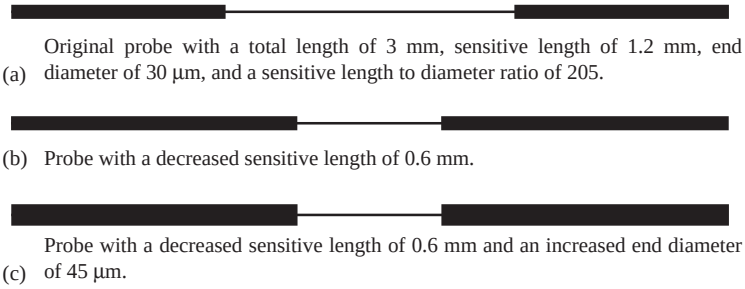

Fig. 8. Wire geometries for (a) the original probe, Probe 3, (b) for a probe with $L_g/L=2$ and $d_g=30\,\mu m$, Probe A, and (c) for $L_g/L=2$ and $d_g=45\,\mu m$, Probe B.

5. Effect of L/d

The previous work had shown that a range of sensitive length-to-diameter ratios between 310 and 160 was acceptable [7]. A combination of changing the total length, and altering the end length to sensitive length ratio can allow a geometry that has a L/d within the acceptable range but still has favourable vibration characteristics. If a length-to-diameter ratio of at least 160 is

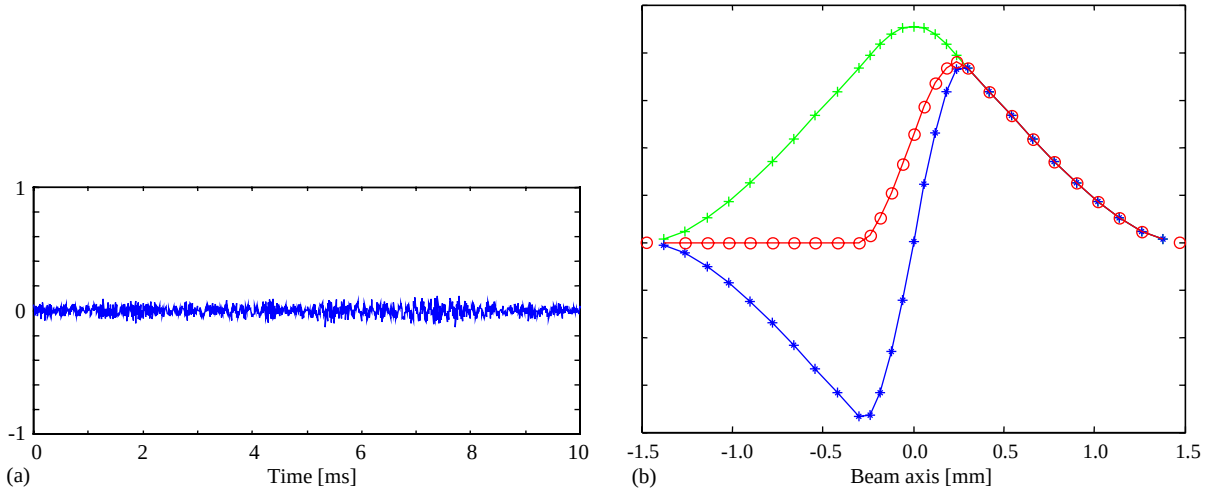

Fig. 9. Showing (a) the displacement history and (b) first (+), second (*) and average (o) mode shapes for Probe C with $d = 3.75\,\mu m$ such that $L/d = 160$.

kept, then a sacrifice of the reduction in response is necessary. However, the length-to-diameter ratio may also be increased by decreasing the sensitive diameter. Such a modification leads to a more flexible sensitive section which vibrates with a larger amplitude. Compensation for this detrimental effect can be achieved by moving to a larger L_g/L than 2. An example shown is for a L_g/L of 3, a total length, L_o, of 3 mm, and end diameter, d_g, of 45 μm (Probe C). Here, the sensitive diameter has been decreased to 3.75 μm, from the original value of 5.75 μm resulting in a L/d of 160. The normalised displacement history for this probe is given in Fig. 9(a) in the same format as in Fig. 7. The reduction in rms amplitude from the Probe 3 amplitude is 85%. Compared to the 90% reduction achieved by ignoring the L/d limit with Probe B, this geometry maintains much of the suggested benefits.

The first three natural frequencies for the wire geometries discussed above are shown in Table 1. Probe 3 has a separation of 1060 Hz between its first and second natural frequencies, and 7520 Hz between its second and third natural frequencies, relative differences of 10% and 40%, respectively. The last probe geometry given in the table, Probe C with a L/d of 160, has a first and second natural frequency separation of only 302 Hz, which is a relative difference of just under 4%.

In Fig. 9(b), the first (+) and second (*) mode shapes and their spatial average (o) are shown for Probe C. The average mode shape is obtained by assuming equal contributions from the first two modes, similar to the case discussed in Fig. 2(c). Approximately, one-third length of the probe on the left side of the averaged mode shape, experiences severely limited magnitudes due to the out of phase nature of the two modes. The right side, on the other hand has comparable magnitudes for all three. Since the second natural frequency is slightly larger than the first, the averaged shape shown here cannot be maintained. In time, the restricted magnitudes of the left side will travel towards right and then back towards left, as the first two mode shapes go out of phase and then go back to being in phase on the right.

Table 1
First three natural frequencies of Probe 3 and the new geometrices

	Natural frequencies (Hz)		
	1	2	3
Probe 3 $L_g/L = 0.77$, $d_g = 30\,\mu m$, $d = 5.75\,\mu m$, $L/d = 205$	9380	10440	17960
Probe A $L_g/L = 2$, $d_g = 30\,\mu m$, $d = 5.75\,\mu m$, $L/d = 104$	5850	7692	35633
Probe B $L_g/L = 2$, $d_g = 45\,\mu m$, $d = 5.75\,\mu m$, $L/d = 104$	8825	9500	53600
Probe C $L_g/L = 2$, $d_g = 45\,\mu m$, $d = 3.75\,\mu m$, $L/d = 160$	7736	8038	48349

6. Experimental details

The geometry of a probe wire is not a standard one to enable comparisons with published results from independent sources. Hence, verification of the numerical predictions must be done experimentally. Due to the small size of a hot-wire probe, a scaled-up experimental model was used for ease in fabrication and measurement. The numerical model discussed in earlier sections was scaled up by 1000 times, making it 3 m long instead of 3 mm. Furthermore, steel and aluminium replaced tungsten and gold for low cost. Therefore, the experimental model was not an exact replica but a close representation of the earlier numerical one. This fact necessitated new numerical predictions with a revised model for comparison with experimental observations.

A total of four beam geometries were chosen here to coincide with the probe wire geometries discussed earlier. Beam 3 is the starting beam geometry, constructed with aluminium ends of 30 mm diameter, with a steel sensitive length of 6 mm. It has a total length L_o, of 3 m, and a sensitive length L, of 1.18 m giving it a L_g/L of 0.77. It is a 1000 times scaled up version of Probe 3. The beam is mounted between two workbench vices bolted into a reinforced concrete floor. This rigid end support provides a reasonable simulation of the built-in boundary condition. The next beam geometry analysed, Beam A, has an end diameter, d_g, of 30 mm, and a L_g/L of 2. The other two beam geometries, Beams B and C, are for end diameters of 45 mm with L_g/L of 0.77 and 2, respectively.

The experimental setup is shown schematically in Fig. 10. The signal generator, item 1, produces a broadband, random signal containing a frequency range up to 50 Hz, sufficient to excite the first three natural frequencies of the beam. This type of excitation is identical to that in the simulations and indicative of turbulent flow. The signal is then amplified, item 2, and sent to the shaker, item 3.

The shaker was consistently mounted at 800 mm from the right-hand side rigid end support, so that it was well away from any nodal positions for the mode shapes under consideration. A soft spring, item 4, was used to transfer the force from the shaker to the beam. The response of the beam was then measured using a laser displacement transducer, item 5. The measurement point was at 1350 mm from the right-hand side rigid end support. As previously mentioned, the mid-

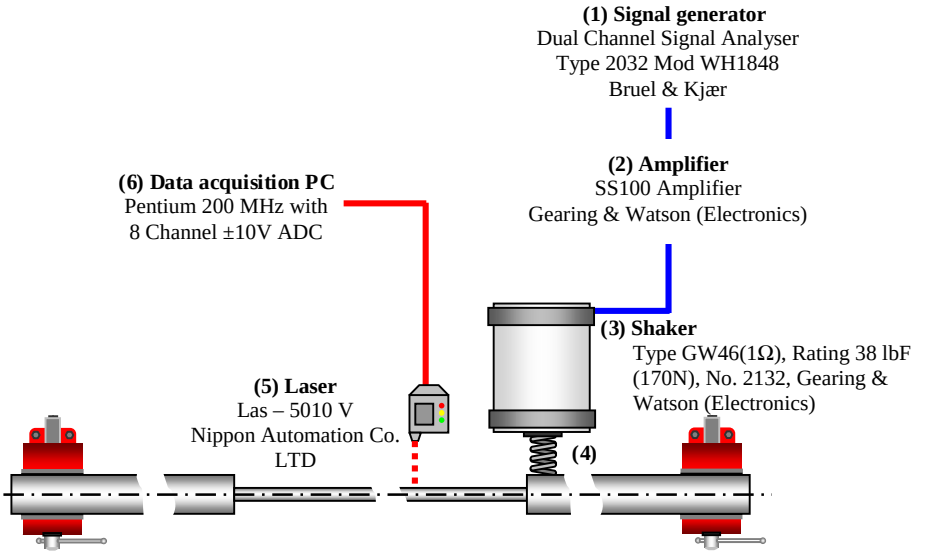

Fig. 10. Schematic representation of the experimental rig showing: (1) the signal generator, (2) the signal amplifier, (3) the shaker, (4) soft spring, (5) the laser displacement transducer and (6) the data acquisition PC.

Table 2
Experimentally and numerically determined natural frequencies of the experimental beams. f_i refers to the ith natural frequency in Hz

	f_1	f_2/f_1	f_2	f_3/f_2	f_3	Normalised rms displacement
Beam 3						
Experimental	13.5±0.5	1.44	19.5±0.5	1.13	22±1	1
(numerical)	(16.5)	(1.45)	(24)	(1.2)	(29)	(1)
Beam A						
Experimental	12.5±0.5	1.36	17±0.5	3.12	53±2	0.63
(numerical)	(13.5)	(1.30)	(17.5)	(3.97)	(69.5)	(0.25)
Beam B						
Experimental	16±0.5	1.5	24±1	1.25	30±1	0.58
(numerical)	(19)	(1.92)	(36.5)	(1.05)	(38.5)	(0.85)
Beam C						
Experimental	21±1	1.08	22±1	2.14	47±2	0.27
(numerical)	(21.5)	(1.05)	(23)	(3.34)	(76.8)	(0.18)

point of the beam was not chosen to avoid the node at the centre point with even modes of vibration.

The displacement data were recorded on a personal computer, item 6, with an analogue to digital converter (ATD) using HP VEE [14]. The data were sampled at a frequency of 1000 Hz for just over 32 s. The maximum frequency of interest was observed to be around 50 Hz, as summarised in Table 2. The data capture commenced after sufficient time was given for the initial transient response to subside. The data were then analysed using Matlab [12].

7. Experimental results

The predicted and measured natural frequencies of the four beams, are shown in Table 2. The odd numbered columns show the natural frequencies, while the even numbered columns, with the exception of the last column, show the ratio, $f_{(i+1)}/f_i$ where i is the mode number. Each row has the experimental results and experimental uncertainty based on repetitions for different beam geometries, followed by the numerically predicted results in parentheses. Some reduction in the magnitude of the natural frequencies is observed experimentally, as compared to those predicted numerically, for all beam geometries analysed. The reason for this apparent reduction in the overall stiffness may be due to not having perfectly rigid end supports experimentally, as is the case numerically.

According to the numerical results, Beams 3 and B are expected to have relatively well separated first and second natural frequencies, f_2/f_1 of 1.45 and 1.92, respectively, making them susceptible to large amplitude vibrations. The experimentally measured separation between the natural frequencies for Beam 3, f_2/f_1 of 1.44, matches the prediction closely. For Beam B, a separation of 1.5 is observed experimentally, not in agreement with the numerically predicted value of 1.92. On the other hand, numerical predictions suggest that Beams A and C have close first and second natural frequencies, f_2/f_1 of 1.30 and 1.05, respectively, making them less susceptible than Beams 3 and B. Experimental observations verify these predictions closely, and Beams A and C have f_2/f_1 of 1.36 and 1.08, respectively.

The forced vibration responses of Beams 3, A, B and C are presented in Figs. 11–14. The Fast Fourier Transform (FFT) of displacement histories is shown in Figs. 11(a), 12(a), 13(a) and 14(a), respectively, for these beams. In each figure, the natural frequencies corresponding to the normal modes are labelled, along with the observed skipping modes. Skipping modes were observed to exist in three dimensions, in a circular orbit around the beam's neutral axis. They were first noticed after obtaining a large number of spectral peaks in the response of the beams under random excitation. When tested under sinusoidal excitation, true normal modes were identified with their characteristic shape. The remainder of the spectral peaks gave a combination of the fundamental mode existing simultaneously in both the horizontal and vertical planes. Although the skipping modes appeared at several distinct frequencies, they retained their shape similar to the in-phase fundamental mode without any nodes.

These three-dimensional skipping modes were thought to exist due to slightly asymmetric boundary conditions where the vertical plane is slightly less rigid than the horizontal one. As a result, any slight misalignment of the forcing from the horizontal plane was able to excite skipping modes. Skipping modes cannot exist numerically. The difference in the numerically and experimentally observed displacement response is therefore attributed largely to the presence of the skipping modes in the experiments.

In Table 2, the last column shows the experimental and numerical normalised rms displacement amplitudes. Numerically, Beam A, due to its close first and second natural frequencies, is expected to have a vibration amplitude reduced by 75% in comparison with that of Beam 3. While the experimental results verify this prediction qualitatively, the reduction in the rms amplitude of Beam A, in comparison with that of Beam 3, is only about 40%. Further differences are seen for Beam B, where a reduction of just over 40% in rms was measured, whereas 15% less rms displacement than that of Beam 3 was predicted numerically. Beam C is the only geometry for

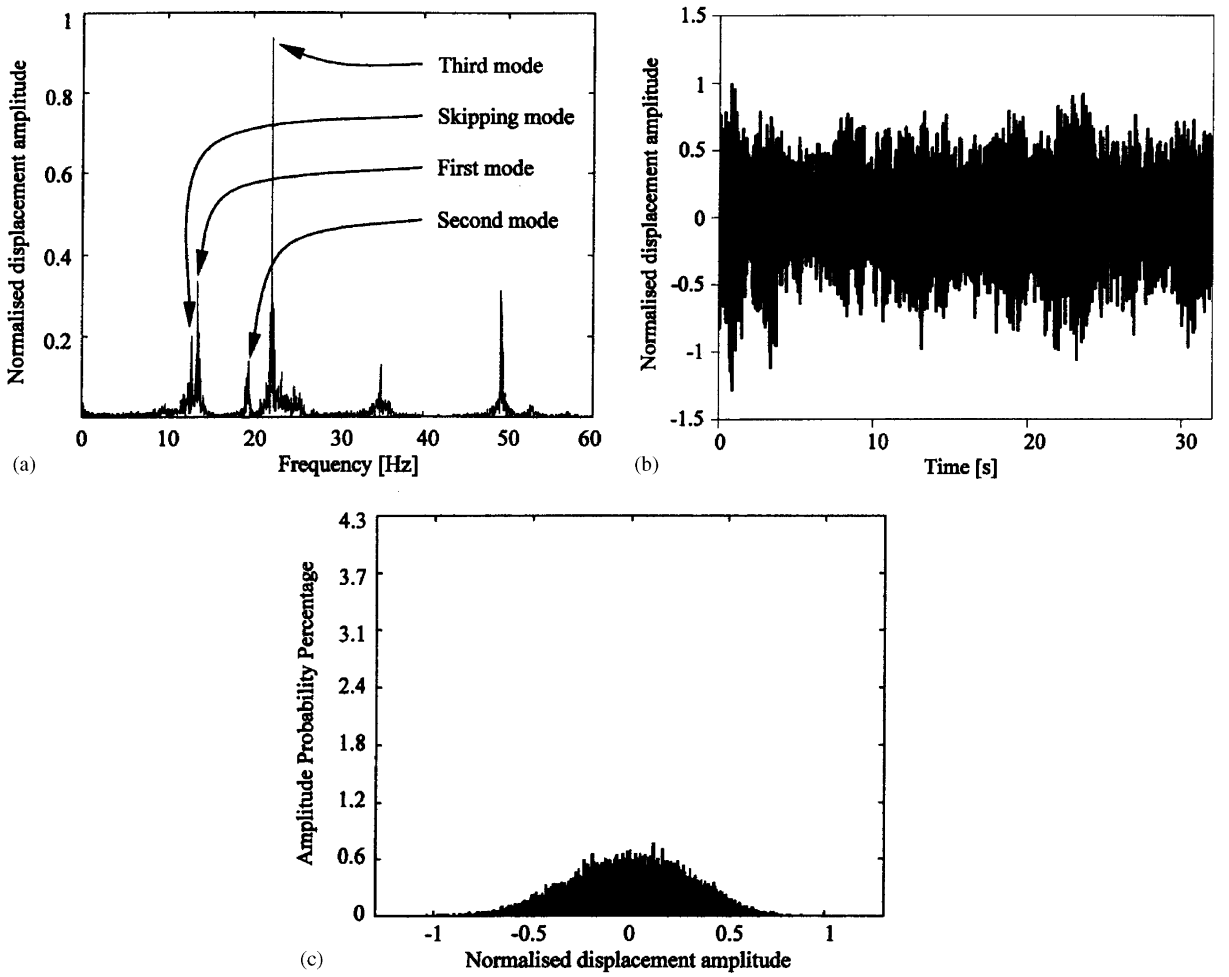

Fig. 11. Beam 3 (a) FFT, (b) displacement history and (c) amplitude probability distribution for the starting beam geometry of $L_g/L = 0.77$ and end diameter, $d_g = 30$ mm.

which the measured and predicted results agree, and about 73% and 82% reduction, respectively, in the rms displacement, is achieved.

The only beam not to exhibit any skipping modes was Beam C, possibly due to its first and second plane modes being almost coincident. This observed result is in agreement with the numerical prediction, since this geometry was predicted to be the least susceptible to large amplitude vibrations. In the experiments, when allowed to vibrate freely in response to a transient input, a node clearly travelled up and down the sensitive length of this beam, as predicted. The beam attempted to have both mode shapes simultaneously. Since the second natural frequency was slightly larger than the first, a travelling node was formed. This travelling node prohibited the natural vibration modes from building to resonance.

Figs. 11(b), 12(b), 13(b) and 14(b) show the normalised displacement histories of the experimentally measured data for each beam. Again, the axes for all four plots are the same, so

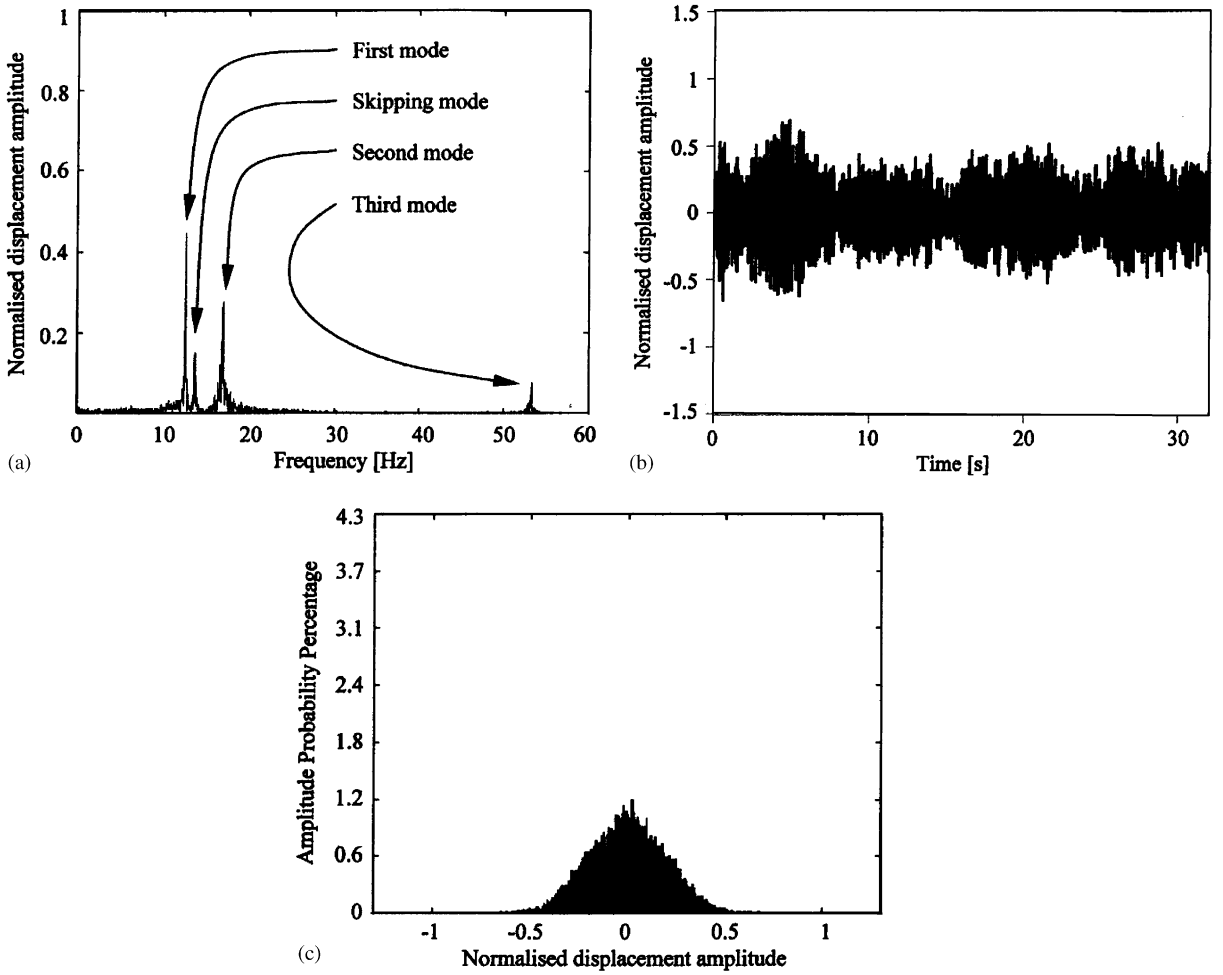

Fig. 12. Same as Fig. 11 but for Beam A with $L_g/L = 2$ and $d_g = 30$ mm.

that comparisons may be easily made. Another form of comparison between each geometries' displacement history is shown with the percentage probability distributions in Figs. 11(c), 12(c), 13(c) and 14(c). The horizontal axis here is the same as the vertical normalised displacement amplitude axis of Fig. 11(b), while the vertical axis is the percentage probability. If the vibration amplitude were always close to zero, such histograms would be tall and narrow. For a beam that is susceptible to large amplitude vibrations, the percentage probability has a shallow and wide distribution. The taller and narrower probability distribution of Beam C in Fig. 14(c) than that of Beam 3 in Fig. 11(c) indicates a significant improvement over Beam 3. Beams A and B, however, show only small improvements over Beam 3.

As indicated earlier, the presence of skipping modes might be the cause of the difference between experimental and numerical results. While the skipping modes are difficult to avoid experimentally, they are completely removed by choosing the geometry of Beam C, which has

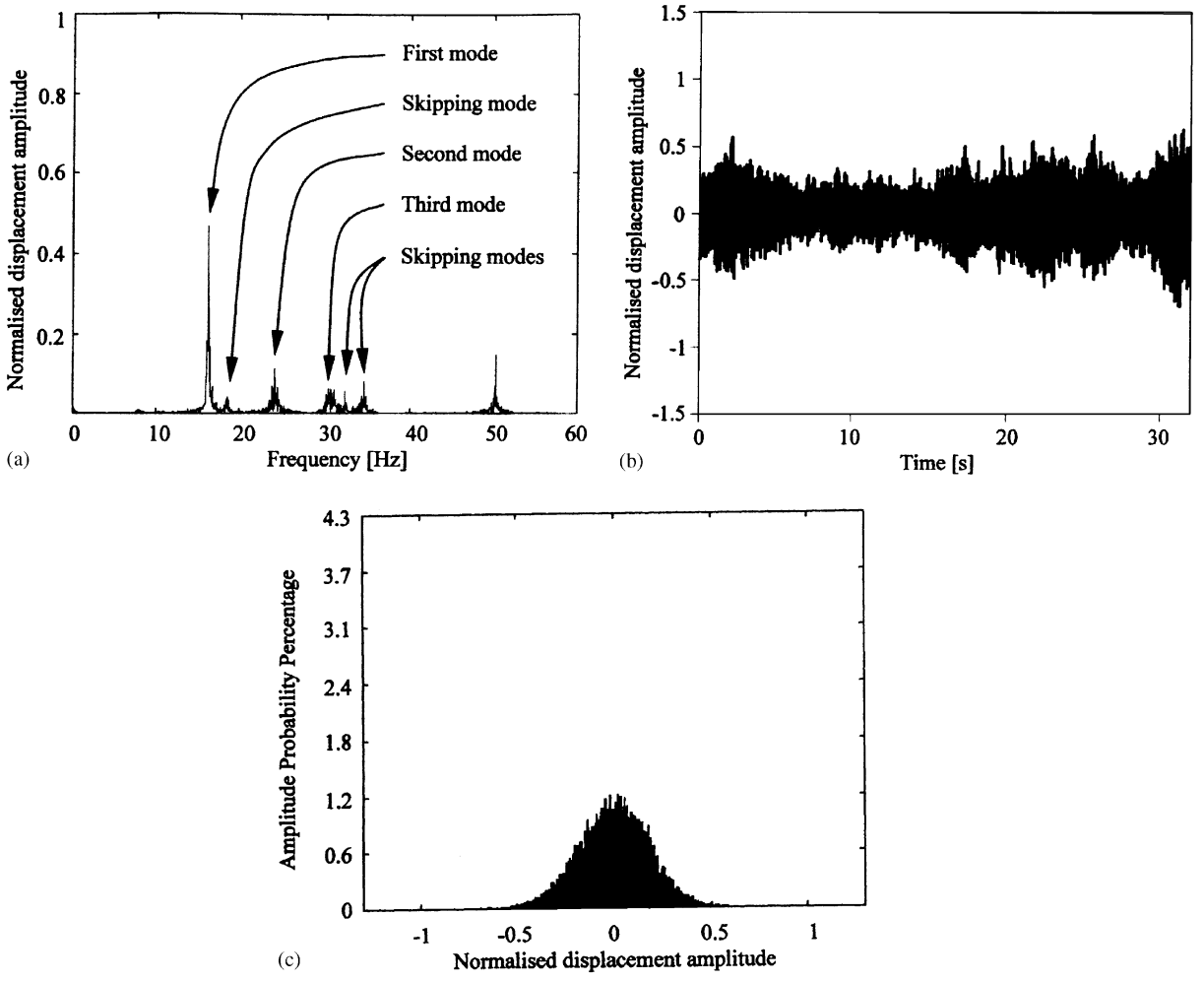

Fig. 13. Same as Fig. 11 but for Beam B with $L_g/L = 0.77$ and $d_g = 45$ mm.

been shown to be more stable than Beam 3 with less than 30% of the rms amplitude. Despite the rather simplistic approach used in the numerical prediction model, it is pleasing to notice that the suggested geometry of Beam C maintains its effectiveness.

8. Conclusions

Numerical results and experimental verification are presented for a novel technique of vibration control using structural modifications. The objective of the structural modifications is to impose coincident modes for slender beam structures. Although it is intuitive to anticipate that the node of a higher mode should restrain the peak magnitude of a lower mode (second and first modes,

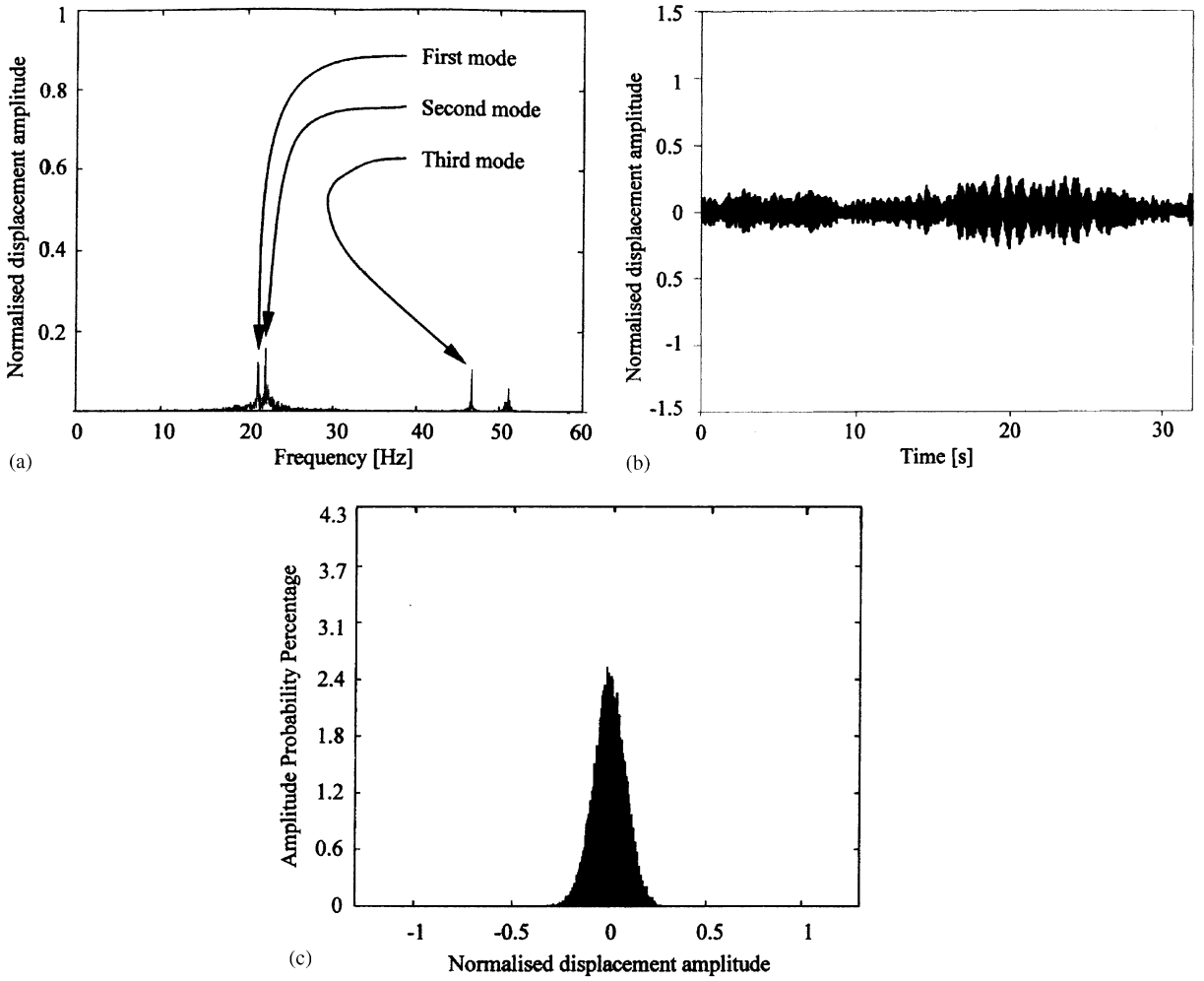

Fig. 14. Same as Fig. 11 but for Beam C with $L_g/L=2$ and $d_g=45\,\text{mm}$.

respectively, in this particular case), the present contribution does not yet extend to predict the achievable level of control.

The particular problem investigated here is that of hot-wire probe vibration under turbulent flow conditions resulting in random excitation of the probe wire. Numerical results indicate that significant improvements are possible if the first two modes are forced to be close. Experimental verification of the numerical results is presented for scaled up slender beams. The next stage in this research is to conduct actual size probe manufacture followed by flow velocity measurements.

Acknowledgements

C.S. Anderson received an Australian Postgraduate Award during the course of this work.

References

[1] Dantec Probes for hot-wire anemometry, Probe Catalogue, 1996.
[2] Ö.F. Turan, S.E. Semercigil, G. Chukkapalli, Effect of structural vibrations on hot-wire probe response, *Measurement Science and Technology* 4 (1993) 1416–1425.
[3] A.E. Perry, G.L. Morrison, Errors caused by hot-wire filament vibration, *Journal of Physics E: Scientific Instruments* 5 (1972) 1005–1008.
[4] A.E. Perry, G.L. Morrison, Vibration of hot-wire anemometer filaments, *Journal of Fluid Mechanics* 50 (1971) 815–925.
[5] F.H. Champagne, Turbulence Measurements with Inclined Hot-wires, PhD Thesis, University of Washington, 1966.
[6] G. Comte-Bellot, Hot-wire anemometry, *Annual Review of Fluid Mechanics* 8 (1976) 209–230.
[7] Ö.F. Turan, R.S. Azad, Effect of hot-wire probe defects on a new method of evaluating turbulence dissipation, *Journal of Physics E: Scientific Instruments* 22 (1989) 254–261.
[8] C.S. Anderson, S.E. Semercigil, Ö.F. Turan, An investigation of the structural dynamics of hot-wire probes, *Proceedings of the 13th Australasian Fluid Mechanics Conference*, Melbourne, Australia, 1998, pp. 75–78.
[9] C.S. Anderson, S.E. Semercigil, Ö.F. Turan, Hot-wire geometry modifications to improve dynamic response, *Third ASME/JSME Joint Engineering Conference*, FEDSM99-7352, San Francisco, CA, 1999.
[10] C.S. Anderson, Ö.F. Turan, S.E. Semercigil, Measurement anomalies due to hot-wire probe vibration, in preparation.
[11] S.S. Rao, *Mechanical Vibrations*, third ed, Addison-Wesley, New York, 1995.
[12] Matlab®, *The Student Edition of Matlab*, Mathworks Inc., Prentice-Hall, Englewood Cliffs, NJ, 1995. Version 5.1.
[13] Ö.F. Turan, R.S. Azad, Comparison of the zero-wire-length dissipation technique with spectral corrections and the effect of high turbulence intensity, *Experimental Thermal Fluid Science* 6 (1993) 292–308.
[14] HP VEE (Hewlett Packard Visual Engineering Environment), Version 4.01.